Interaction and percolation in the *L*64 triblock copolymer micellar system

Laurent Lobry
Dipartimento di Fisica, Universitá di Messina, and Istituto Nazionale per la Fisica della Materia, Sezione di Messina, Vill. S. Agata, CP 55, 98166 Messina, Italy

Norberto Micali
Istituto di Tecniche Spettroscopiche del CNR, Via La Farina, Messina, Italy

Francesco Mallamace,* Ciya Liao, and Sow-Hsin Chen
Department of Nuclear Engineering, 24-209 Massachusetts Institute of Technology, Cambridge, Massachusetts 02139-4307
(Received 23 April 1999)

We present results of analyses of an extensive set of static light scattering (SLS), small angle neutron scattering (SANS), and viscoelastic (frequency dependent complex moduli) measurements of aqueous solutions of a triblock copolymer micellar system. We investigate Pluronic *L*64 ($PEO_{13}PPO_{30}PEO_{13}$)-water system in a wide range of composition and temperature. We determine phase diagram of the disordered micellar phase, including a cmc-cmt curve, a cloud point curve, the critical concentration, and the critical temperature by means of SLS and SANS. The microstructure and interaction between micelles are determined by analyses of SANS intensities. SANS intensity distributions are well described by combining the cap-and-gown model for the polymer segmental distribution within a micelle and the sticky hard sphere model for the intermicellar structure factor. The existence of percolation loci at well defined poins in the temperature-concentration plane is inferred from an abrupt increase of the stickiness parameter extracted from SANS data and from two order of magnitude jump of the complex moduli at the percolation point. Study of temperature dependence of real (storage) and imaginary (loss) part of the complex modulus at fixed concentration and frequency lends further support to the existence of a percolation line. We observe an increase of some order of magnitude of the real and imaginary part of viscosity at certain temperature and composition, a phenomenon usually ascribed to a gelation process in a polymer solution. The definitive confirmation of the percolation process is obtained by frequency dependent complex viscosity measured in a frequency range 0–160 (rad/sec). From these measurements we clearly observe a well defined frequency scaling behavior of the complex moduli and a loss angle (δ) independent of the frequency. Scaling exponents, determined for frequency-dependent complex moduli satisfy the scaling relations predicted by the scalar elasticity percolation theory. [S1063-651X(99)02112-1]

PACS number(s): 61.25.Hq, 61.12.Ex, 82.70.Dd, 83.70.Hq

I. INTRODUCTION

Polyethylene oxide (PEO) polypropylene oxide (PPO) containing block copolymers represent a class of polymers that associate spontaneously in aqueous solutions [1]. In particular, a series of symmetric triblock copolymer composed of $(PEO)_m$-$(PPO)_n$-$(PEO)_m$ has been synthesized as polymeric surfactants that have wide range of commercial applications including detergency, emulsification agent, lubricant, drug encapsulation, and cosmetics [2,3,4]. This class of triblock copolymers is available commercially under a trade name ''Pluronic'' from BASF [2]. The self-association of Pluronics is characterized by sensitivity to temperature but insensivity to concentration [4,5–11], at least within the disordered micellar phase, that are an ideal characteristics as a candidate for the existence of a percolation phenomenon. We have been studying a particular Pluronic surfactant family containing 40% (by molecular weight) of PEO and 60% of PPO. This Pluronic family has several members, namely, *P*104, *P*94, *P*84, *L*64, and *L*44, in decreasing order of molecular weight. They all form spherical micelles in water within certain ranges of temperatures and polymer concentrations [3,4,7,10]. These micelles are heavily hydrated (about 50% water). We have previously studied three members *P*104, *P*84, and *L*44 using light (SLS) [12] and neutron scattering (SANS) [13] techniques and have arrived at reasonably accurate models for the polymer segmental distribution in a micelle and the intermicellar interaction potential.

In this paper, we shall describe a new series of studies focusing our attention exclusively on $L64/D_2O$ system using combined techniques of static light scattering (SLS), small angle neutron scattering (SANS) and rheology. Our main aim is to give a complete phase diagram within the disordered micellar phase and show experimentally the existence of both a critical consolute point and a percolation line in this system.

II. EXPERIMENT

Samples were prepared at room temperature by dissolving *L*64 copolymer in deuterated water without further purification. The polymer concentrations in solution was expressed in weight percent ($C = \mathrm{wt}\,\%$). Pluronic *L*64 was obtained

*Permanent address: Dipartimento di Fisica, Università di Messina, and Istituto Nazionale di Fisica della Materia, Sezione di Messina, Vill. S. Agata, CP 55, 98166 Messina, Italy.

from BASF and deuterated water (purity 99.9%) from Aldrich. The samples were stored at room temperature for a few days before measurements for stabilization and to ensure a complete aggregation equilibrium was reached. Temperature of the samples was controlled to an accuracy of 0.2 °C. Samples used in optical studies (SLS light scattering) have been filtered before measurements by a Millepore filter having a pore size of 0.2 μm. All sample solutions appeared transparent and homogeneous. Light scattering measurements were performed at least 1 h after the filtration to ensure a complete aggregation equilibrium. The same batch of *L*64 copolymer was used to carry out all experiments.

A. Light scattering

Static light scattering (SLS) measurements were performed in a range of scattering angles $20° \leqslant \theta \leqslant 150°$, corresponding to magnitudes of the scattering wave vector in the range $5.6\,\mu\mathrm{m}^{-1} \leqslant k \leqslant 31.4\,\mu\mathrm{m}^{-1}$ $[k=(4\pi/\lambda)n_0 \sin(\theta/2)$, where n_0 is the index of refraction of D_2O]. The light source for SLS was the 5145 Å line of an argon laser operating at a power level of 50 mW. We used an optical scattering cell of a diameter 1 in., thermostated within ± 10 mK in a refractive index matching bath. We have also measured the sample turbidity to check multiple scattering effects and to have a rough estimation of the surfactant aggregation and phase separation.

An absolute cross section measurement was performed using an intensity calibration standard of benzene [Rayleigh scattering cross section per unit volume, $R_{\mathrm{benzene}}=1.184 \times 10^{-5}\,\mathrm{cm}^{-1}$ $(\lambda=6328\,\text{Å})$]. The calibration constant was thus determined experimentally in order to convert the photo detector count rate into an absolute scattering intensity which is the Rayleigh ratio. To determine the phase diagram of the disordered micellar phase, including the cmc-cmt curve, the cloud point curve, the critical concentration and the critical temperature, we scanned a wide temperature (10–70 °C) and concentration $[C(\mathrm{wt}\%)=0.002-0.25]$ ranges. More precisely, using light scattering and turbidity measurements, we have studied the following concentrations: C=0.002, 0.003, 0.005, 0.01, 0.02, 0.03, 0.05, 0.06, 0.07, 0.1, 0.15, 0.2, 0.25. To characterize the polymer micellar system with light scattering we have also measured the refractive index increment (dn/dC) of the solution as functions of the polymer concentration and temperature [14,15].

The normalized scattering intensity showed, in the covered angular range, no angular dependence since the micellar sizes are much smaller compared with the probe wavelength. On this basis, we have considered, for the data analysis, only the scattering intensities obtained at scattering angle $\theta = 90°$. It is well known [14] that, in polymeric solutions, the amplitude and shape of absolute scattering intensity of light (or neutrons) vs concentration contain information on the self-aggregation phenomenon, average molecular weight, the cmc-cmt curve, the volume fraction and on the interaction parameters. For the treatment of the our data on copolymer micellar solutions, we adopt a recently proposed method [12] that extends the method of Zimm plot and take into account effects due to higher concentrations. It has been shown that such a method is particularly appropriate for Pluronic polymeric micellar solutions.

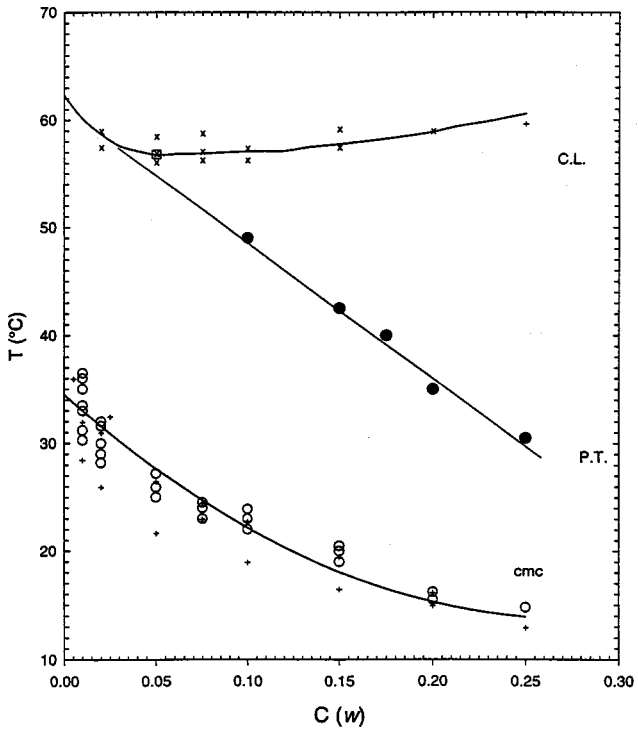

FIG. 1. The phase diagram of Pluronic L64 in D_2O determined by SLS. The phase diagram includes: the cmc-cmt curve (cmc), the cloud point curve (CL), the critical concentration and critical temperature (square). The percolation line is indicated as PT. Dots in the cmc-cmt curve are the results from turbidity measurements.

With such a procedure for analyses of the SLS data we have studied the system $L64/D_2O$ and determine its phase diagram, shown in Fig. 1. The phase diagram includes: the cmc-cmt curve, the cloud point curve, the critical concentration and the critical temperature. With the same procedure we have also determined: the molecular weight, the aggregation number and micellar hydration. From the latter quantity we obtain a relation between the micellar volume fraction ϕ and the weight concentration c the relationship $\phi \cong 2c/\rho$, where ρ is the density of the copolymer solution which is very close to unity. Turbidity data (dots in Fig. 1) agrees with these scattering measurements.

B. Neutron scattering

Small angle neutron scattering (SANS) experiments were performed at ORNL using a 30 m SANS spectrometer. We used an average wavelength $\lambda = 5.75$ Å with a relative wave length spread $\Delta\lambda/\lambda = 10\%$ at sample to detector distances (SDD) of 1.5 and 10 m, respectively, to cover a magnitude of the wave vector transfer range $0.008\,\text{Å}^{-1} < Q < 0.30\,\text{Å}^{-1}$. For all measurements, 1 mm spaced flat quartz cells were used. Samples were loaded to the scattering cells at room temperature. They were preheated in a separate water bath for hours before being moved into the spectrometers for SANS measurements. Temperature of samples was controlled to an accuracy of 0.1 °C. In SANS experiments the use of deuterated water as the solvent enhances the contrast between the micelle, which are made up largely of protonated polymers and some hydrated solvent molecules, and

TABLE I.

Species	Chem. formula	Mol wt.	Mol vol ($Å^3$)	Scattering lengths $\Sigma\Sigma\Sigma\Sigma b_i$(fm)	Scattering length dens (10^{-6} $Å^2$)
EO	$—(CH_2)_2O—$	44	72.4	4.14	0.572
PO	$—(CH_2)_3O—$	58	95.4	3.31	0.347
solvent	D_2O	20	30.3	19.153	6.321
*L*64	$PEO_{13}PPO_{30}PEO_{13}$	2884	4744	206.9	0.437

the solvent. The magnitude of scattering densities of the polymer segments and the solvent and their numerical values are listed in Table I.

Measured intensities were corrected for the background and empty cell contributions and normalized by intensities of a standard polymer sample. The absolute intensity was expressed in unit of scattering cross section per unit sample volume $I(Q)$ (in unit of cm^{-1}). A FORTRAN code based on gradient searching nonlinear least-squares fitting method was used to fit the absolute SANS intensities to a theory. We used a theory recently developed by Liu, Chen, and Huang [13] for analyzing Pluronic *P*85 and *P*104 copolymer micellar solutions.

C. Viscoelastic measurements

Viscoelastic measurements were performed with a Haake CV 100 rheometer using a stainless steel couette geometry cell. The instrument was used in an oscillatory mode. The chosen frequency range was $9.24\times10^{-2}<\omega(\mathrm{rad/sec})<64$. As it is well known, the rheological properties of a viscoelastic system are characterized by the dynamical complex viscosity η^* and by the complex shear modulus [16]:

$$G^*=G'+iG''=i\omega\eta^*=i\omega(\eta'+\eta'') \tag{1}$$

where G' and G'' are, respectively, the storage and the loss modulus. Usually η^* depends on the shear rate $\dot{\gamma}$ and G^* on the frequency ω. In our oscillatory experiment the storage and the loss shear moduli, G' and G'', have been obtained from the measurement of the time dependence of the stress, σ, by using the definition [16]: $\sigma=\gamma_0(G'\sin\omega t+G''\cos\omega t)$ where γ_0 is the amplitude of the strain and $\delta(\omega)$ the phase angle between the stress and strain, measured with a condition that the amplitude $\sigma_0(\omega)$ of the stress varies as $\sigma=\sigma_0\sin(\omega t+\delta)$. On this basis we have $G'=(\sigma_0/\gamma_0)\cos\delta$, $G''=(\sigma_0/\gamma_0)\sin\delta$, and $G'/G''=\tan\delta$.

III. RESULTS AND DISCUSSION

A. Phase diagram

Recent SANS measurements performed in triblock copolymer micelles in aqueous solutions (Pluronic *P*84 and *P*104) [13] give definitive indication that the scattered intensity distributions at higher temperatures can be described satisfactorily by taking into account an additional intermicellar interaction that has a form of a surface adhesion, besides the known excluded volume effect represented by a finite size hard core. The origin of the surface adhesion is the interpenetration of polymer chains and the consequent deplection of the solvent in the corona region when two micelles come into contact. At higher temperatures, water becomes a poor solvent to PEO chains due to a decreasing probability of forming hydrogen bonds with oxygen atoms in the polymer chains. On this basis the SANS intensities has been satisfactorily fitted, over the entire disordered micellar range, in an absolute scale by an adhesive hard sphere model of Baxter [17]. In this model, the pair potential, $u(r)$, between micelles is written as

$$\frac{u(r)}{k_BT}=\begin{cases}\infty & \text{for} \quad 0<r<R' \\ -\Omega & \text{for} \quad R'<r<R, \\ 0 & \text{for} \quad R<r,\end{cases} \tag{2}$$

where $R-R'$ is the thickness of the adhesive surface layer.

To obtain the interparticle structure factor $S(Q)$ from the interparticle potential $u(r)$, Baxter solved Ornestein-Zernike (OZ) equation [18] in Percus-Yevik (PY) approximation [19] in the limit that the thickness of the adhesive layer goes to zero but the adhesive potential tends to infinity in such a way that one can introduce a finite stickiness parameter $1/\tau$ defined as $1/\tau=12\exp(\Omega)(R-R')/R$. We shall call this special limit a ''sticky sphere'' model. Baxter also used the PY approximation to solve the OZ equation to first order in the fractional surface layer thickness $\varkappa=(R-R')/R$. One of the relevant features of the Baxter model is that, by using the liquid theory [20], the phase diagram (including the percolation line) of the sticky sphere system can be analytically derived. From the equation of state one finds the existence of a gas-liquid phase transition with a critical point occurring at a micellar volume fraction $\phi_c=0.1213$ and stickiness parameter $1/\tau_c=10.25$. Figure 2 shows the complete phase diagram, theoretically obtained according to the Baxter model. The figure gives locations of one and two phase regions, spinodal line, percolated and nonpercolating regions in a plane defined by τ_c/τ and ϕ_c/ϕ.

From the comparison of the measured phase diagram (Fig. 1) with the one corresponding to a Baxter system, we infer that for Pluronic *L*64, there is a well defined critical point and a percolation line. Therefore we wish to explore such properties by means of SANS and rheological measurements. From SANS, as will be shown in next section that, by using a structure model for the micelle developed previously by Liu *et al.* [12] in combination with the Baxter model for the intermicellar correlation, to calculate the scattering cross section of the micellar solution. The result of fit of the theory to the measured SANS intensity profile allows evaluation of the stickiness parameter in a given phase point. The sticky parameter approaches values larger than unity in the percolation region, whereas it approaches a value close to 10 near the critical point along a critical isochore. In addition we will

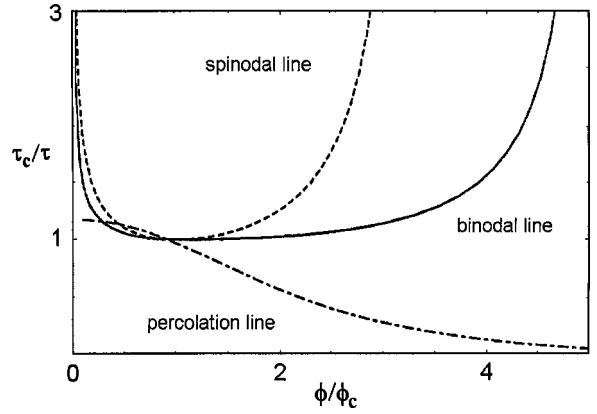

FIG. 2. The phase diagram, theoretically obtained from Baxter's model [see Chen *et al.*, J. Phys.: Condens Matter **6**, 10 855 (1994)]. The figure gives locations of one and two phase regions, the spinodal line, the percolated and nonpercolating regions in a plane defined by τ_c/τ and ϕ/ϕ_c.

use SLS intensity to gain information on location of the critical point.

Percolation phenomena (or the sol-gel transition typical of polymeric solutions) can also be characterized experimentally from the study of mechanical quantities such as complex viscosity or the corresponding moduli [21–23]. More precisely, from the experimental point of view, a micellar solution in the phase below percolation can have a finite value of shear viscosity while in the phase above the threshold it is characterized by a very high viscosity. Such a situation is already reflected in the theoretical models [24,25]. In fact in the percolation theory due to Stauffer, he considers that below percolation (in the sol phase), only finite molecules are present, while above the percolation (in the gel phase), a macroscopic molecule, infinite in spatial extent, coexists with the finite molecules [24]. In addition, on considering the frequency dependence of the complex viscosity, a percolating system in the vicinity of the threshold, must exhibit a marked transition from a simple liquid medium to an elastic medium [22]. These properties has been in the past observed in many percolating systems, such as polyacrylamide cross-linked gels [26], epoxy resins [27], pectin [28], branched polymers [29], and colloidal solutions [30] that are systems very similar to the actual *L*64 micellar system under study.

Figure 3 shows results of oscillatory shear measurements for the system $L64/D_2O$ at $C=0.2$ and 0.25, as a function of temperature measured at a frequency of 1.36 rad/sec. At all

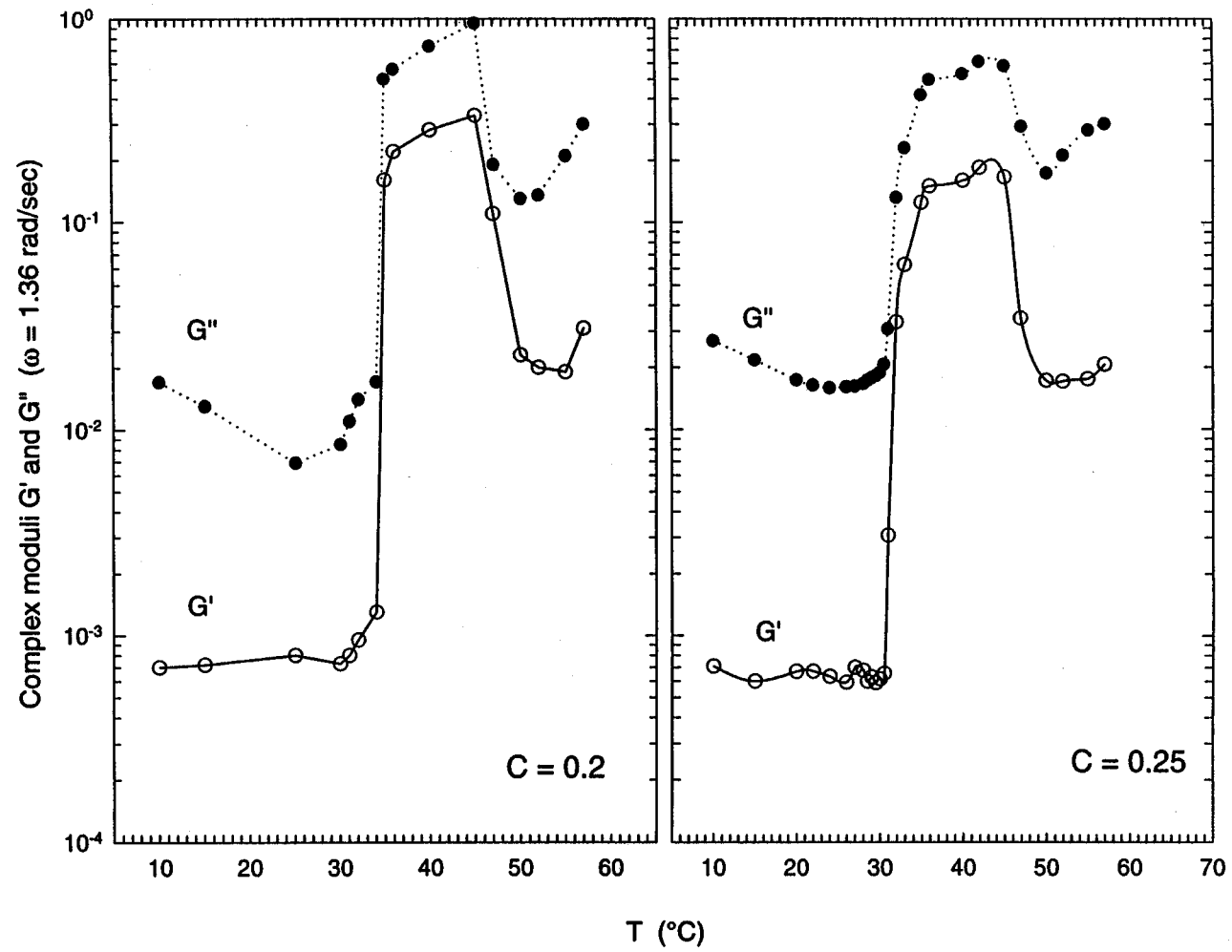

FIG. 3. Viscoelastic properties of $L64/D_2O$, at polymer weight fractions $C=0.2$ and 0.25, as a function of the temperature at 1.36 rad/sec. G' and G'' are the storage and the loss moduli (measured in Pascal), respectively. Notice sharp rises of the moduli at percolation temperatures.

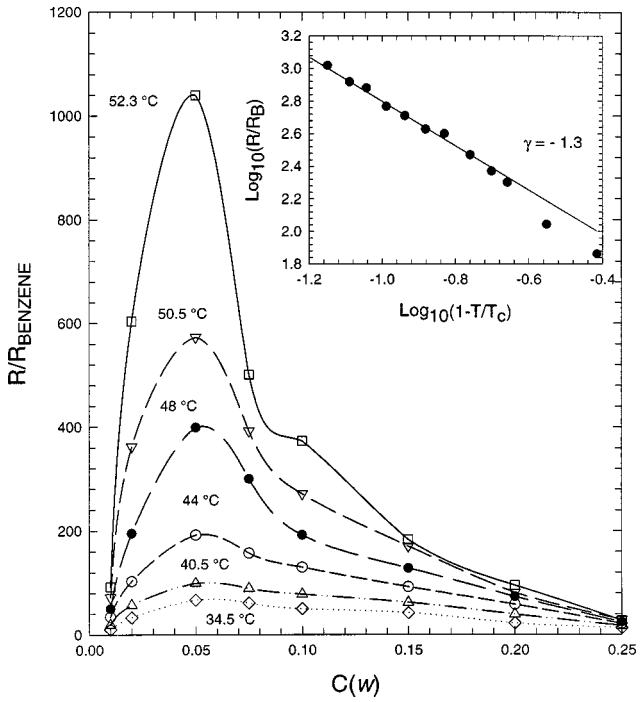

FIG. 4. Normalized scattered light intensities (R/R_{benzene}), measured at $\theta=90°$, as a function of concentration at six different temperatures, $T=34.5$, 40.5, 44, 48, 50.5, and 52.3 °C. Lines connecting data points are a guide for eyes. Inset: The log-log plot of normalized light scattering intensity versus $(T-T_c)/T_c$, along an iso-concentration line, $C=0.05$ ($\phi\simeq 0.1$), $T_c\simeq 57.16$ °C is estimated from SANS data, taken along the critical isochore ($C=0.05$). Solid line is the best fit of the intensity data that gives the critical power-law index $\gamma=1.3\pm 0.03$.

the temperatures behavior of a viscoelastic liquid is observed, since $G''>G'$ [16]. Around 35 °C (for $C=0.2$) and 31 °C (for $C=0.25$) both moduli increases abruptly about two order of magnitude (with an increase in the elastic storage modulus larger than the loss modulus). This shows that the overall behavior is analogous to the one observed in a sol-gel transition driven by temperature: a viscous solution changes to a gel-like state with increasing temperature. For higher temperatures (about 50 °C) a new viscoelastic fluid is formed. We have studied such a transition for five different concentrations ($C=0.1$, 0.15, 0.17, 0.2, and 0.25) and we have reported the corresponding sol-gel transition temperatures in the phase diagram shown in Fig. 1. As can be observed, the resultant transition line, in the shear moduli, is very similar, in the temperature-concentration plane, to the percolation locus defined by the sticky sphere model (Fig. 2). Such a result constitutes a direct evidence for a percolating phenomenon in these triblock copolymer micellar solutions. Additional indication come from analyses of SANS results and the frequency dependence of the rheological quantities.

To investigate the criticality of the system we consider the results of SLS intensities as a function of temperature and concentration. Figure 4 reports the normalized light scattered intensities (R/R_{benzene}), measured at $\theta=90°$, as a function of concentration at temperatures 34.5, 40.5, 44, 48, 50.5 and 52.3 °C (the related lines are a guide for eyes). As can be seen, there is a marked maximum that increases its value with increasing T, located at about $C=0.05$ ($\phi\simeq 0.1$), near the critical volume fraction predicted by Baxter model [17,20]. Micellar suspensions are systems in which the onset of the critical effects can be detected many degrees from the critical temperature [31]. The intensity is proportional to the diverging osmotic compressibility χ [32]. It is well known that the isothermal osmotic compressibility varies according to $\chi=\chi_0[(T-T_c)/T_c]^{-\gamma}$. From SANS data, taken along the critical isochore (Fig. 5), we have estimated that $T_c\simeq 57.16$ °C. Therefore, a log-log plot of the intensity data corresponding to $C=0.05$ versus $(T-T_c)/T_c$ have been used to obtain the critical index γ. Such a plot is shown in the inset of Fig. 4 and the obtained value of γ ($\gamma=1.3\pm 0.03$) agrees with theory and the ones measured in analogous systems [31].

B. Small angle neutron scattering analysis

The absolute scattered intensity $I(k)$ of a system of monodispersed spheres can be written in terms of a product of the normalized particle structure factor $\tilde{P}(k)$ and the interparticle structure factor $S(k)$. For a micellar system it is written as [33,13]

$$I(k)=cN\left[\sum_i b_i-\rho_w v_m\right]^2\tilde{P}(k)S(k), \tag{3}$$

where c is the polymer concentration (number of polymer molecules per milliliter), N is the aggregation number of a micelle, and the term within the square bracket is the contrast factor [33]. The first term of this latter quantity is the sum of coherent scattering lengths of atoms comprising of the polymer molecule, ρ_w the scattering length density of the solvent and v_m the polymer molecular volume. It should be noted that in Eq. (7) the absolute intensity is proportional to the aggregation number N. The polymer concentration and the contrast factor are known quantities.

Figures 5 and 6 show two series of SANS intensity distributions of the micellar system Pluronic $L64/D_2O$ at $C=0.05$ and $C=0.2$, respectively, for different temperatures. It is important to note that the first one is a concentration very near the critical one. The corresponding spectra show the temperature effect: on approaching the critical region scattering intensities increase with a marked narrowing in their forward peaks.

For data analysis of SANS intensity distributions we used a recently proposed method that have given a satisfactory description of the structure and thermodynamics of micellar system made of Pluronic polymers in aqueous solutions [13]. In this method the particle structure factor is calculated according to a ''cap and gown'' model for the microstructure of the micelle, taking into consideration the polymer segmental distribution and the water penetration profile in the core and corona regions. The intermicellar structure factor is calculated using a sticky hard sphere model which takes into account a temperature dependent short-range attraction between micelles that is necessary to lead to the phenomena of percolation and critical opalescence in addition to a basic hard core.

The particle structure factor $P(k)$. The cap-and-gown model combines both characteristic features of a diffuse distribution of polymer chains in the outer layer of the micelle

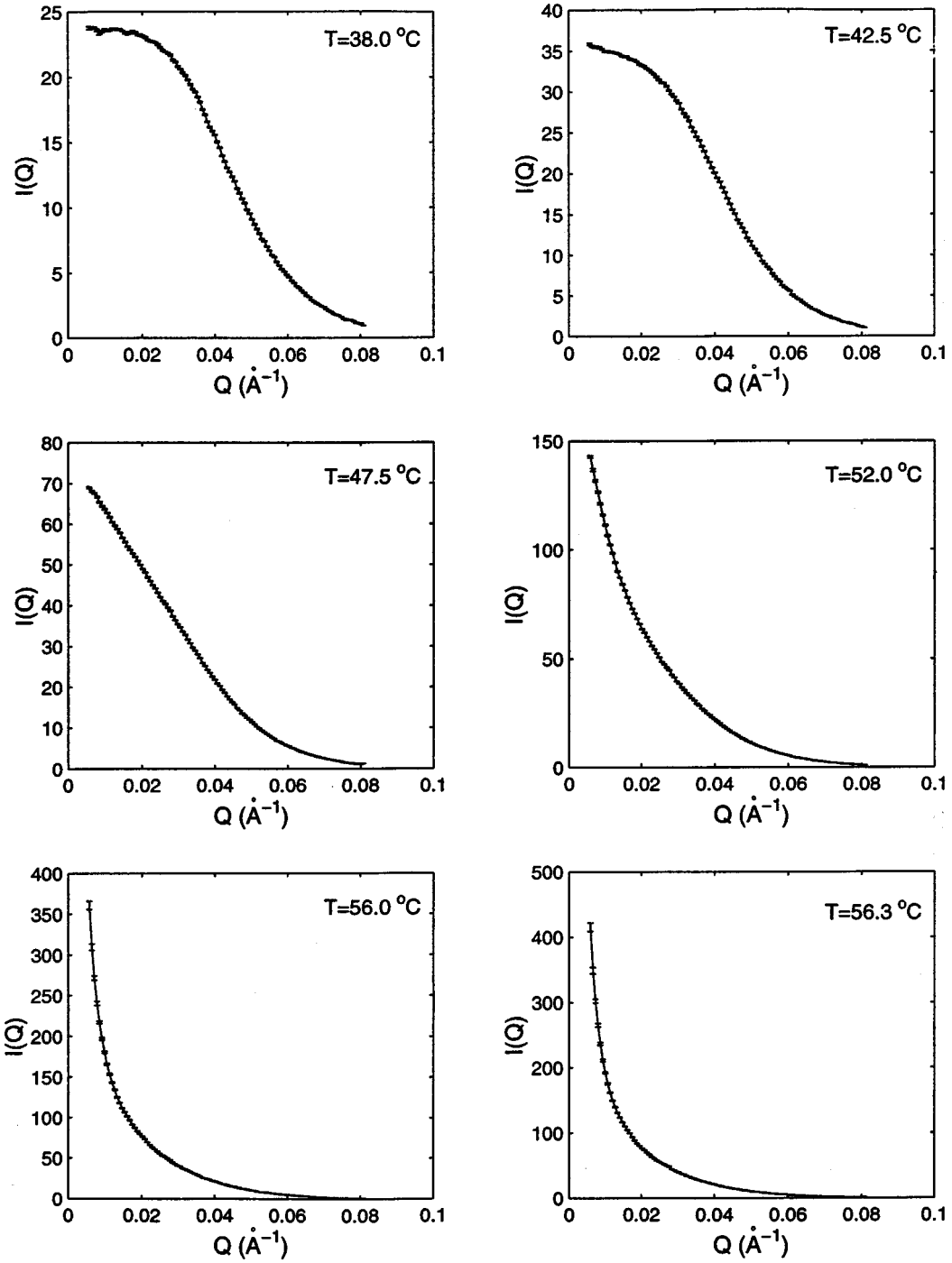

FIG. 5. SANS intensity distributions $I(Q)$ for $L64/D_2O$ micellar solutions taken along a concentration $C=0.05$ at 38, 42.5, 47.5, 52, 56, 56.3 °C. $C=0.05$ is a concentration very near the critical one. On approaching the critical temperature, scattering intensities increase with a marked narrowing in their forward peaks.

and a global core-shell structure of the particle. It is assumed a Gaussian distribution of the polymer segments in the corona region. The inner core of a micelle is composed of mostly segments which are relatively incompatible with solvent molecules and thus likely to be those of PPO. The outer shell, on the other hand, accommodates polymer segments that are compatible with the solvent and, therefore, are mostly PEO. The outer shell is also called the corona region, has a more diffuse polymer segmental distribution. Such a structure represents a micelle formed by triblock copolymers of the PEO-PPO-PEO type in water adequately. In fact the micellar core of low polarity is composed of mostly PPO blocks surrounded by the more polar region composed mostly of PEO blocks. In the cap-and-gown model it is assumed that the radial segmental distribution in the core region starts out uniform within a radius a; it is jointed to a Gaussian distribution with a radius σ.

The neutron scattering length density profile can be calculated in terms of scattering length densities of polymer, ρ_p and water, ρ_w (known quantities) as

$$\rho(r)=\phi_w(r)\rho_w+\phi_p(r)\rho_p, \tag{4}$$

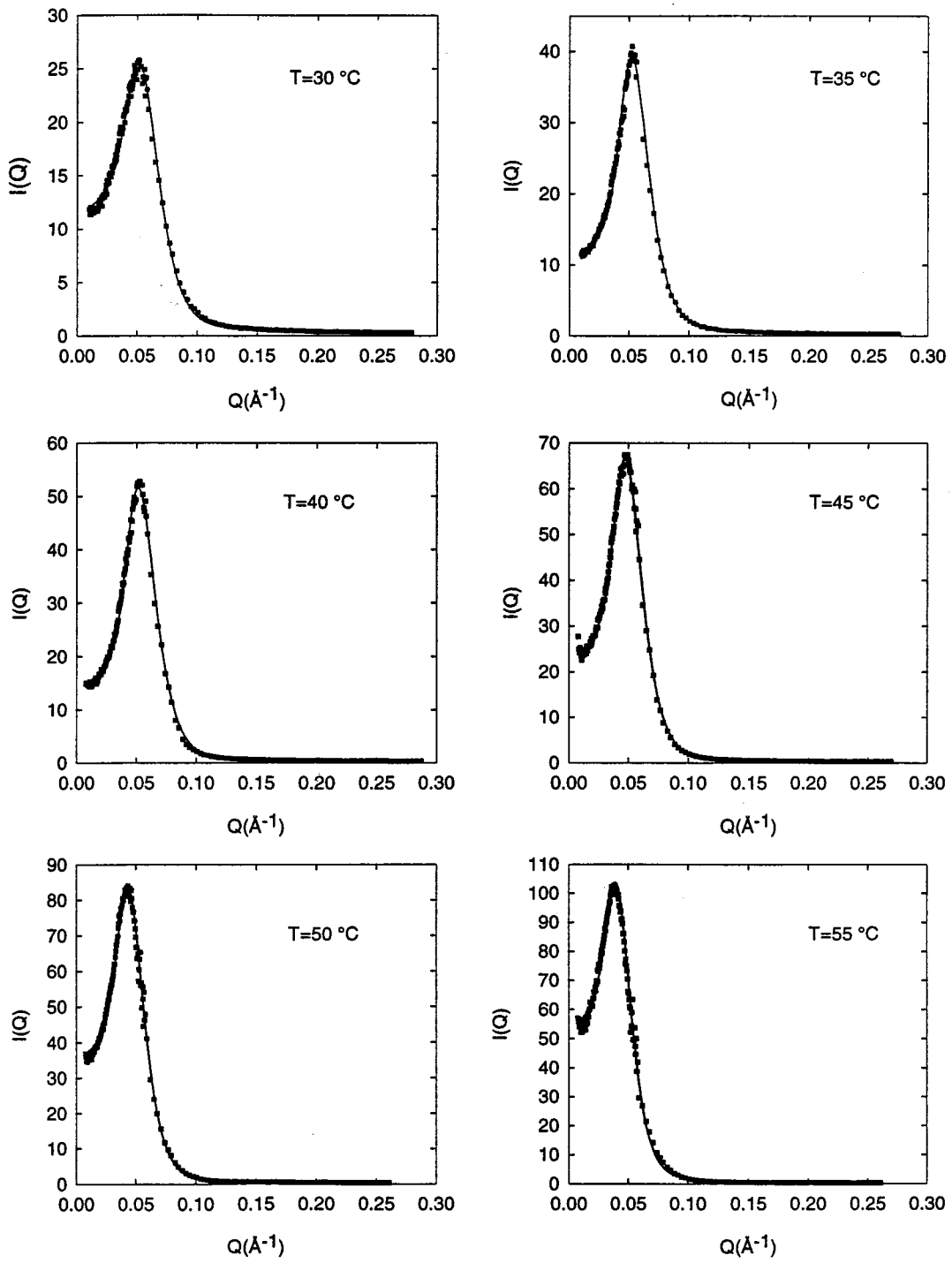

FIG. 6. SANS data in an absolute scale along an isoconcentration line, $C=0.2$, at a series of temperatures, 30, 35, 40, 45, 50, 55 °C and their fits. Symbols are SANS data and solid lines are fits. The fits in absolute scale use a sticky hard sphere model of Baxter for the interparticle structure factor and a cap-and-gown for the form factor.

where $\phi_w(r)$ and $\phi_p(r)=1-\phi_w(r)$ are the volume fraction occupied by water molecules and the volume fraction occupied by the polymer segments, respectively, at a radial distance r from the center of a spherical micelle. The difference between the actual scattering length density at r and that of the solvent (the contrast)

$$\Delta\rho(r)=\rho(r)-\rho_w=[\rho_p-\rho_w]\phi_p(r) \tag{5}$$

is the quantity which determines the particle form factor $F(k)$.

The cap-and-gown model assumes that the polymer volume fraction is distributed as

$$\phi_p(r)=\begin{cases}\phi_p & \text{for} \quad 0<r<a,\\ \exp\left(-\dfrac{r^2}{\sigma^2}\right) & \text{for} \quad a<r<\infty,\end{cases} \tag{6}$$

where the volume fraction of water in the core is $\phi_{\text{core}}=1-\phi_p$. The core radius a, the Gaussian width σ and the polymer volume fraction in the core ϕ_p are related by a geometrical constraint.

From the Fourier transform of the contrast $\Delta\rho(r)$ we obtain the particle form factor, $F(k)$

$$F(k)=\int \Delta\rho(r)\exp(i\vec{k}\cdot\vec{r})d^3r. \tag{7}$$

Thus the normalized form factor $\tilde{F}(k)$ is given by

$$F(k)=N\left(\sum_i b_i-\rho_w v_m\right)\tilde{F}(k), \tag{8}$$

where

$$\tilde{F}(k)=\frac{v_{\text{PPO}}}{v_{\text{PEO}}+v_{\text{PPO}}}\left[\frac{3j_1(ka)}{ka}+\frac{3}{\phi_p}\int_1^{\infty}\frac{\sin(kax)}{ka}\times\exp(-t^2x^2)xdx\right]. \tag{9}$$

v_{PEO} and v_{PPO} are molecular volumes of the PEO and PPO parts of the polymer. The normalized particle structure factor is given by $\tilde{P}(k)=|\tilde{F}(k)^2|$.

Interparticle structure factor $S(k)$. Liquid theory gives methods by which the interparticle structure factor $S(k)$ of a system of interacting spheres is determined by a given interparticle interaction potential $u(r)$. The starting point is the relation between the direct correlation function $c(r)$ and the net correlation function $h(r)$ expressed by an OZ equation [18]

$$h(r)=c(r)+\rho\int d\vec{r}\,'c(r')h(|\vec{r}-\vec{r}'|), \tag{10}$$

where ρ is the particle number density. The net correlation function $h(r)$ is related to the radial distribution function $g(r)$ by $h(r)=g(r)-1$. For given T, ρ, and $u(r)$, the OZ equation may be solved under various approximations for the functions $h(r)$ and $c(r)$. For hard spherelike systems, the so-called Percus-Yevic (PY) approximation [19] is known to be most accurate. Baxter used the PY approximation to solve the OZ equation analytically to the first order in the fractional surface layer thickness $(R-R')/R$ [17]. The solution can be expressed in terms of the following set of parameters [34] for a given volume fraction ϕ and the surface stickiness $1/\tau$:

$$\Gamma=\frac{\phi(1+\phi/2)}{3(1-\phi)^2}, \tag{11}$$

$$\Delta=\tau+\frac{\phi}{1-\phi}, \tag{12}$$

$$\lambda=\frac{6(\Delta-\sqrt{\Delta^2-\Gamma})}{\phi}, \tag{13}$$

$$\mu=\lambda\phi(1-\phi), \tag{14}$$

$$\alpha=\frac{(1+2\phi-\mu)^2}{(1-\phi)^4}, \tag{15}$$

$$\beta=-\frac{3\phi(2+\phi)^2-2\mu(1+7\phi+\phi^2)+\mu^2(2+\phi)}{2(1-\phi)^4}. \tag{16}$$

Denoting by Q a dimensionless parameter ($Q=kR$, the product of the wave vector k and the outer particle diameter R), the interparticle structure factor $S(Q)$ of the sticky hard sphere system [$\varkappa\to 0,\Omega\to\infty$ in such a way that $1/\tau=12\exp(\Omega)\varkappa$ remains finite] can then be written in a closed form as [34]

$$\frac{1}{S(Q)}-1=24\phi\left[\alpha f_2(Q)+\beta f_3(Q)+\frac{1}{2}\alpha\phi f_5(Q)\right]+2\phi^2\lambda^2 f_1(Q)-2\phi\lambda f_0(Q), \tag{17}$$

where the various functions are defined as

$$f_0(x)=\sin x/x,$$

$$f_1(x)=(1-\cos x)/x^2,$$

$$f_2(x)=(\sin x-x\cos x)/x^3,$$

$$f_3(x)=[2x\sin x-(x^2-2)\cos x-2]/x^4,$$

$$f_5(x)=[(4x^3-24x)\sin x-(x^4-12x^2+24)\cos x+24)]/x^6.$$

The hard sphere limit is recovered by setting $1/\tau\to 0$ and $\lambda\to 0$.

Having the normalized structure factor $\tilde{P}(k)$ calculated from the cap-and-gown model and the interparticle structure factor $S(k)$ from the sticky hard sphere model, the absolute intensity $I(k)$ [Eq. (7)] can then be calculated. The fitting parameters are the aggregation number N, the total hydration number H (number of water molecules attached to a polymer in a micelle), stickiness $1/\tau$, outer micellar diameter R, and polymer volume fraction in the core ϕ_p. Other parameters, such as the volume fraction of micelles ϕ, core radius a, Gaussian distribution width σ, and the hydration number in the core and shell, are deduced quantities. The sensitive parameters of the fit are N, H, and R. The aggregation number determines the overall amplitude of the scattered intensity and can be obtained by fitting SANS data in an absolute scale. The total hydration number determines the volume fraction of micelles which controls the peak height of the structure factor $S(k)$. The micellar diameter determines the peak position of $S(k)$. These three parameters basically determine the general shape and amplitude of $I(k)$. Away from the critical region the stickiness $1/\tau$ and ϕ_p determine the detailed rise and fall of the interaction peak and the small and large k behaviors of the scattered intensity. In the critical region, the stickiness parameter controls the rise of scattering intensity at $k=0$ (Ornstein-Zerniche scattering function); it therefore is a sensitive parameter as one approaches the critical point. As can be observed from Fig. 5 and 6 the quality of the fits is uniformly excellent for the system of *L*64 triblock copolymer micelles in the entire range of disordered micellar phase. As an example, parameters characterizing the micro-

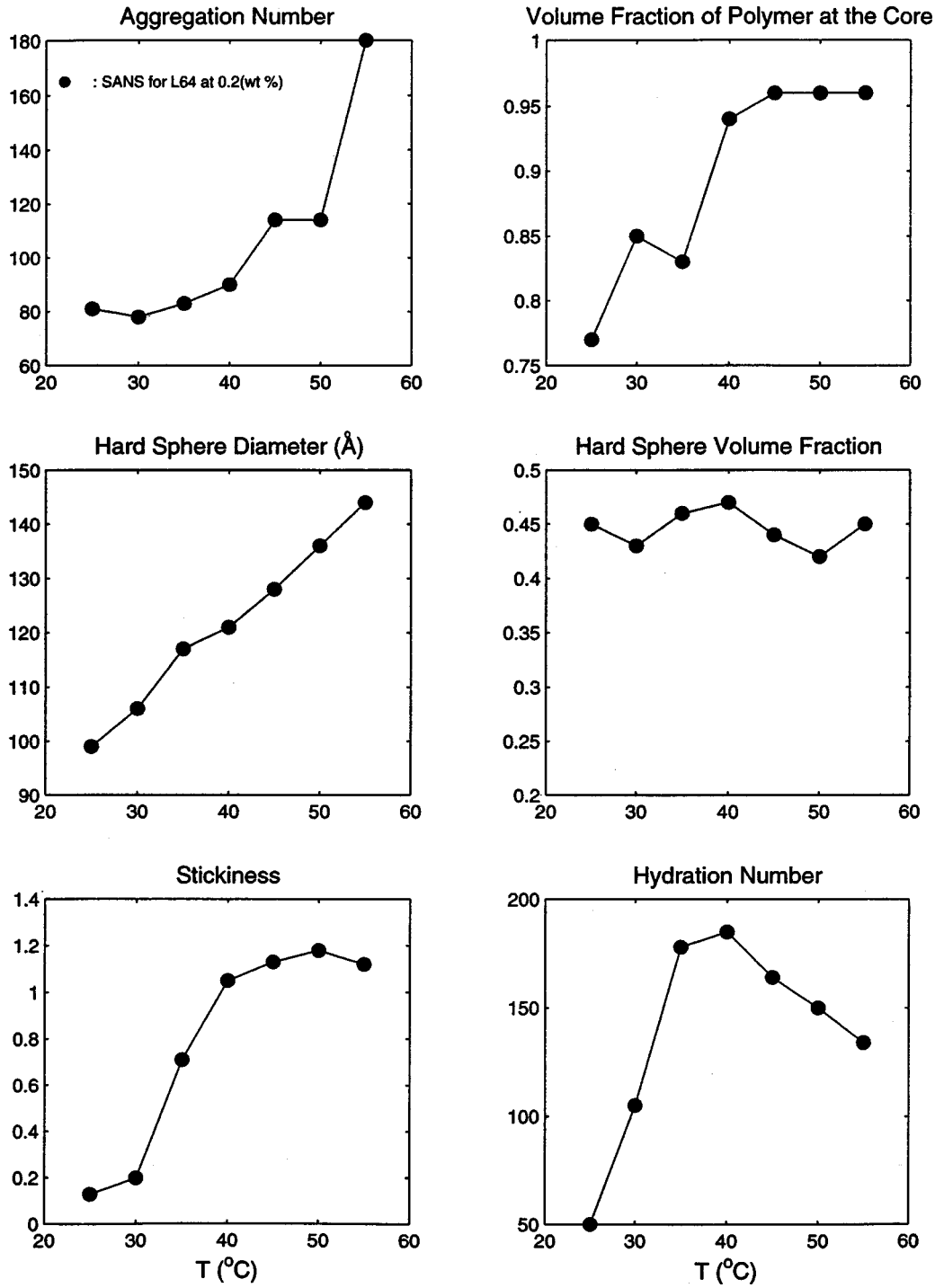

FIG. 7. Parameters for the microstructure and interaction of $L64/D_2O$ polymeric micelles, at a fixed concentration ($C=0.2$) and different temperatures, extracted form SANS data by using the sticky sphere model for the structure factor and the cap and gown for the form factor.

structure and interaction of $L64$ polymeric micelles thus obtained, for fixed concentration ($C=0.2$) and different temperatures, are shown in Fig. 7. We find that the aggregation number and the diameter of the micelle increase with temperature. The volume fraction of polymer in the core, and hydration number increase with temperature only in the range 20–40 °C, whereas for higher temperatures these quantities show little variation. This agree with the main results of micellar solution of the same family of polymer, Pluronic $P84$ and $P104$, previously studied by SANS using the same analysis procedure [13]. For the aim of the present work the relevant data obtained is temperature variation of the stickiness parameter as can be seen in Fig. 7. This quantity is characterized by different values at low and high temperatures, At low temperatures the stickiness of micellar surface indicates that the micelles are close to hard spheres. The surface of micelles become more and more stickier just in the temperature region for which viscoelasticity (Fig. 3) indicates a percolation transition. Fits to the absolute intensities along the critical concentration ($C=0.05$) show a large increase in stickiness with temperature up to a value ($1/\tau=10$) at the highest temperature ($T=56.3\,°C$) studied. Such

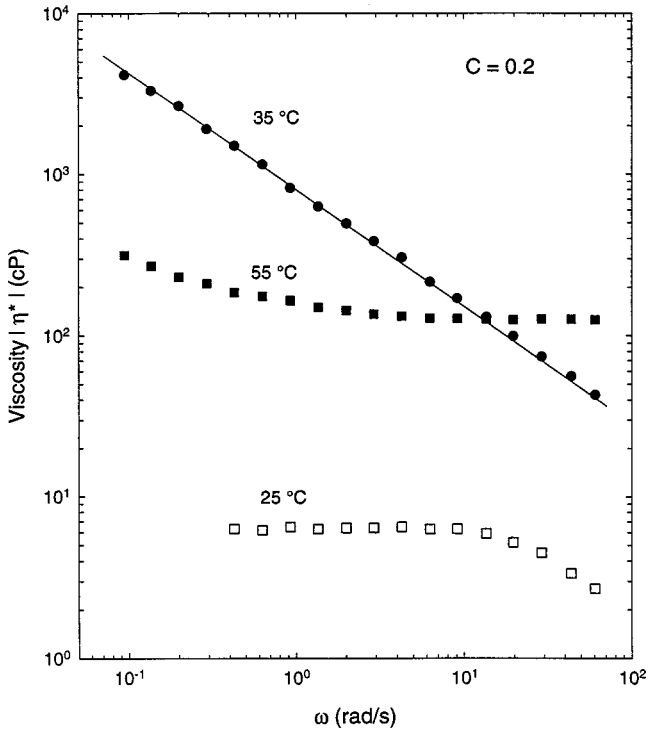

FIG. 8. Log-log plot of measured complex viscosity $|\eta^*|$, as a function of the frequency, for the $L64/D_2O$, micellar system at a fix concentration $C=0.2$ but three different temperatures, 25, 35, and 55 °C. The straight line for data at $T=35$ °C shows clearly a power-law behavior of $|\eta^*|$ vs ω.

a result is in complete agreement with the theoretical prediction [20].

C. Percolation and viscoelasticity

To have a definitive confirmation on the percolation phenomenon in the micellar system under study, we consider frequency dependence of its rheological quantities. In Fig. 8 we show viscosities $|\eta^*|$ of $L64/D_2O$ system as a function of frequency, in a log-log plot, at three different temperatures (25, 35, and 55 °C) at a concentration $C=0.2$. It can be easily seen, the system shows completely distinct behaviors at the three temperatures. At low temperature (25 °C), the viscosity has a frequency dependence of a colloidal suspension [35]. For $T=35$ °C, a linear scaling relation of $|\eta^*|$ in ω is observed. For $T=55$ °C, the system transforms into a phase characterized by a high shear viscosity ($\sim 150\,cP$) and a weak viscoelasticity.

Theory of percolation applied to complex fluids (polymers, gels, colloids, etc.) predicts a universal scaling behavior [23,24,36]. An important step for theory of viscoelasticity in a percolating system was the recognition [21,25] that the elastic modulus of a gel and the viscosity of a sol are directly related to the conductance of a random resistor network and a random superconducting network. According to this analogy, the complex modulus $G^*(p,\omega)$ is expected to obey the very same behavior as the AC conductivity of a resistor-capacitor random mixture. Let p be the parameter that controls the percolation transition (may be the cross-linker concentration, the volume fraction of polymers molecules, the temperature, etc.) and p_c its value at the percolation threshold. Then for $\varepsilon=|(p-p_c)/p_c|\ll 1$, the percolating structure is characterized by a correlation length that scales as $\xi \sim \varepsilon^{-\nu}$ and a relaxation time τ, which scales as $\tau \approx \xi^z \approx \varepsilon^{\bar{z}}$, where ν, z and $\bar{z}=\nu z$ are critical exponents [23].

The exponents used to describe viscoelasticity singularities near p_c in the static regime are s,t and Δ [24,25] defined respectively by the following scaling relations:

$$\eta_0 \approx \varepsilon^{-s} \tag{18}$$

and

$$G_0 \approx \varepsilon^{-t}, \tag{19}$$

where G_0 is the static elastic modulus or, more precisely, the elastic modulus of monomers at some microscopic time scale $\tau=\omega_0^{-1}$. At the percolation threshold G' and G'' have the following power-law dependence on frequency ω:

$$G' \approx G'' \approx \omega^{\Delta}. \tag{20}$$

A general scaling form [25,37] has been postulated (by analogy of percolating viscoelasticity with conductivity of a random mixture of conductors) for G^* in the limit when $\omega,\varepsilon \to 0$. In percolating systems the variation of the mechanical properties is correctly described by the form

$$G^*(\omega,\varepsilon)=G_0\varphi^{\pm}(i\omega/\omega_0), \tag{21}$$

$$\omega_0 \approx \xi^{-z} \approx \varepsilon^{\bar{z}}. \tag{22}$$

At low frequencies $\omega \ll \omega_0 \varepsilon^{s+t}$, is for $p \to p_c^-$ $(p<p_c)$

$$\varphi^-(i\omega/\omega_0)=B^-(i\omega/\omega_0)+C^-(i\omega/\omega_0)^2 \tag{23}$$

and for $p \to p_c^+$ $(p>p_c)$

$$\varphi^+(i\omega/\omega_0)=A^+ + B^+(i\omega/\omega_0) \tag{24}$$

at intermediate frequencies $\omega_0 \varepsilon^{s+t} \ll \omega \ll \omega_0$

$$\varphi^-(i\omega/\omega_0) \approx \varphi^+(i\omega/\omega_0)^{\Delta}. \tag{25}$$

This leads to the correct frequency dependence for the elastic (viscous part) G' (G'') for $\omega \to 0$ [Eq. (25)]. Below the percolation threshold $G' \approx \omega^2$ $(G'' \approx \omega)$, very above PT $G' \approx$ const $(G'' \approx \omega)$. With

$$\eta_0 = \lim_{\omega \to 0} G^*(\omega)/\omega \tag{26}$$

the general scaling form leads to the relations between the scaling exponents

$$\bar{z}=s+t \quad \text{and} \quad \Delta=t/\bar{z}=t/(s+t). \tag{27}$$

In this frequency regime, the frequency power-law of the complex modulus G^* has a remarkable consequence: G''/G' have an universal critical value.

More precisely, considering that in rheology the loss angle δ is defined by the relation, $\tan\delta=G''/G'$, one has

$$\delta_c=\frac{\pi}{2}\Delta=\frac{\pi}{2}\frac{t}{t+s}. \tag{28}$$

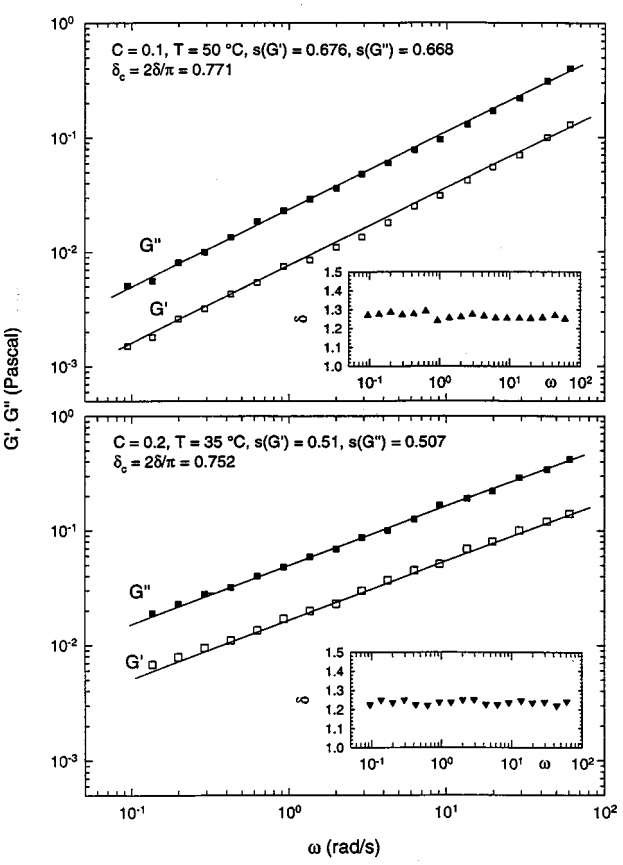

FIG. 9. Log-log plots of the measured storage moduli G' and loss moduli G'' as a function of frequency in the frequency range $9.24\times10^{-2}<\omega(\mathrm{rad/sec})<64$. For $L64/D_2O$. Pluronic micellar solutions at two different concentrations, $C=0.1$ and 0.2. The insets of the figures give the respective values of the loss angle δ as a function of frequency.

The exponents s and t have been calculated numerically by computer simulations giving the values [38] $s=0.75\pm0.04$, and $t=1.94\pm0.1$, so that $\Delta=0.72\pm0.04$.

Figure 9 shows, in a log-log plot, the variation of the storage modulus G'' and the loss modulus G'' in the entire frequency domain studied for two different concentrations, $C=0.1$ and 0.2. In this representation, G' and G'' appear linear in the frequency range 0.0924 to 64 rad/sec, spanning almost three decades. The linear behavior observed confirms that the domain of T and ω investigated is located in the percolation region. The insets of the figures show values of the loss angle δ as a function of frequency, from which Δ $(=2\delta/\pi)$ can also be calculated. It is interesting to observe that the loss angle remains constant (i.e., G''/G' is constant) as a function of ω for the concentrations studied. Continuous lines represent least-square fits to the experimental data of G' and G''. From their slopes we obtain, at the different copolymer concentrations, the following results: for $C=0.1$ we have $\Delta(G'')=0.68\pm0.02$, $\Delta(G'')=0.67\pm0.02$ and $\Delta(\delta)=0.77\pm0.03$, whereas for $C=0.2$, their values are $\Delta(G')=0.51\pm0.02$, $\Delta(G'')=0.51\pm0.02$, and $\Delta(\delta)=0.75\pm0.03$. The values of $\Delta(\delta)$ obtained from the loss angle data can be, in the present experiment, overestimated. This is related to the use of a high value of strain amplitude γ_0 (80% of the viscometer strain amplitude). Such a choice is due to the primary interest in an accurate measurement of the G' and G'' values.

The overall results for the concentration $C=0.1$: scaling in moduli and values of the percolation indices are in complete agreement with theory of static percolation phenomenon. Whereas for $C=0.2$, we observe the same scaling in G' and G'' with ω, but the values of critical indices are different from that of the theoretical model. Such a situation has also been observed in other complex systems. For example, in cross-linking gels [26–28], experimental results have given values of Δ that are close to 2/3 when gels are prepared with the minimum amount of cross-linkers necessary to reach the gel point. In the presence of excess cross-linker at gel point, smaller exponents, approaching $\Delta=0.5$, are sometimes observed. This latter results on percolation indices ($\Delta=1/2$ for $C=0.2$) could be considered as a mean field (or an effective medium theory) results. We have already considered this argument in a separate work [39]. To have a complete and definitive insight on the percolation behavior of the system at high concentrations ($0.4<C<0.6$) an experiment is actually in progress in our laboratory.

We conclude by observing that data on the frequency dependence of viscoelastic behavior of the triblock copolymer micellar system presented here give definitive evidence of the existence of a percolation line in the phase diagram as suggested by a theory based on Baxter's model of sticky hard spheres.

IV. CONCLUSION

We have presented evidence for the existence of an attractive component in the intermicellar interaction which increases as one approaches the cloud point curve. The presence of the critical point and the percolation line in the phase diagram demands a component of short range attractive potential. A quantitative measure of the attraction can be given in terms of the stickiness parameter $1/\tau$ deduced from SANS intensity analysis. The origin of the attraction is the overlapping of the PEO segments on the surface of the micelles when they come into contact. Since as temperature increases water becomes a poorer solvent for the polymer segments, displacement of the solvent as a result of micellar contacts tends to lower the free energy. We intend to investigate the critical scattering along different iso-concentration lines using SANS and DLS in the future. It would be of interest to also investigate the percolation phenomenon in other members of the 40% PEO pluronic family.

ACKNOWLEDGMENTS

We would like to acknowledge the assistance of Dr. Sungmin Choi and Dr. Jah-Shiong Lin in making SANS measurements. We are grateful to Dr. George Wignall of ORNL for giving us neutron beam time in HIFR of ORNL. The research at MIT is supported by a grant from Materials Science Division of US DOE. The research at University of Messina is supported by the MURST-PRIN97 project.

[1] B. Lindman, A. Carlsson, G. Kalstrom, and M. Maltensen, Adv. Colloid Interface Sci. **32**, 183 (1990).
[2] *Pluronic And Technical Brouchure Tetronic Surfactant*, BASF Corp., Parsipanny, NJ, 1989.
[3] P. Alexandridis, V. Athanassiou, S. Fukuda, and T. A. Hatton, Langmuir **10**, 2604 (1994); P. Alexandridis and T. A. Hatton, Colloids Surface **96**, 1 (1995).
[4] C. Z. Zhou and B. Chu, J. Colloid Interface Sci. **126**, 171 (1988); B. Chu, Langmuir **11**, 414 (1995).
[5] D. Wanka, H. Hoffmann, and W. Ulbricht, Macromolecules **27**, 4145 (1994).
[6] E. W. Brown, K. Schillen, M. Almgren, S. Hvidt, and P. Behadur, J. Phys. Chem. **95**, 1850 (1991); K. Schillen, W. Brown, and R. M. Johnsen, Macromolecules **27**, 4825 (1994).
[7] K. Mortensen, J. Phys.: Condens. Matter **8**, A103 (1996).
[8] K. Mortensen, Prog. Colloid Polym. Sci. **91**, 69 (1993); K. Mortensen, W. Brown, and E. Jorgensen, Macromolecules **27**, 5654 (1994).
[9] H. M. Almgren, J. Alsins, and P. Behadur, Langmuir **7**, 446 (1991); M. Almgren, W. Brown, and S. Hvidt, Colloid Polym. Sci. **273**, 2 (1995).
[10] Q. F. Grieser and C. J. Drummond, J. Phys. Chem. **92**, 5580 (1988).
[11] E. B. Jorgensen, S. Hvidt, W. Brown, and K. Schillen, Macromolecules **30**, 2355 (1997).
[12] Y. C. Liu, S. H. Chen, and J. S. Huang, Macromolecules **31**, 6226 (1998).
[13] Y. C. Liu, S. H. Chen, and J. S. Huang, Macromolecules **31**, 2236 (1998).
[14] B. Chu, *Light Scattering—Basic Principle and Practice*, 2nd ed. (Academic Press, San Diego, 1991).
[15] P. J. Flory, *Principles of Polymer Chemistry* (Cornell University Press, Ithaca, NY, 1953).
[16] J. D. Ferry, *Viscoelastic Properties of Polymers* (Wiley, New York, 1980).
[17] R. J. Baxter, J. Chem. Phys. **49**, 2770 (1968).
[18] L. S. Ornestein and F. Zernike, Proc. Acad. Sci. Amsterdam **17**, 793 (1914).
[19] J. K. Percus and G. J. Yevik, Phys. Rev. **110**, 1 (1958).
[20] See, e.g., S. H. Chen, C. Y. Ku, and Y. C. Liu, in *The Physics of Complex Systems*, edited by F. Mallamace and H. E. Stanley (IOP, Amsterdam, 1997), pp. 243–281.
[21] P-G. de Gennes, *Scaling Concepts in Polymer Physics* (Cornell University Press, Ithaca, NY, 1979).
[22] M. Doi and S. F. Edwards, *The Theory of Polymer Dynamics* (Clarendon, Oxford, 1986).
[23] D. Stauffer, *Introduction to Percolation Theory* (Taylor and Francis, London, 1985).
[24] D. Stauffer, Phys. Rep. **54**, 1 (1979).
[25] P-G. de Gennes, J. Phys. (France) Lett. **37**, L1 (1976); C. R. Seances, Acad. Sci., Ser. B **286**, 131 (1979).
[26] C. Allain and L. Salome, Macromolecules **20**, 2957 (1987).
[27] J. E. Martin, D. Adolf, and J. P. Wilcoxon, Phys. Rev. Lett. **61**, 2620 (1988).
[28] M. A. V. Axelos and M. K. Kolb, Phys. Rev. Lett. **64**, 1457 (1990).
[29] D. Durand, M. Delsanti, M. Adam, and J. M. Luck, Europhys. Lett. **3**, 297 (1987).
[30] J. E. Martin, Phys. Rev. A **36**, 3415 (1987).
[31] J. Rouch, A. Safouane, P. Tartaglia, and S. H. Chen, J. Chem. Phys. **90**, 3756 (1989).
[32] P. C. Hohenberg and B. I. Halperin, Rev. Mod. Phys. **49**, 435 (1977).
[33] M. Kotlarchyk and S. H. Chen, J. Chem. Phys. **79**, 2461 (1983).
[34] Y. Liu, S. H. Chen, and J. S. Huang, Phys. Rev. E **54**, 1698 (1996).
[35] I. M. De Schepper, H. E. Smorenburg, and E. G. D. Choen, Phys. Rev. Lett. **70**, 2178 (1993).
[36] J. Essam, Rep. Prog. Phys. **43**, 833 (1980).
[37] A. L. Efros and B. I. Shkolovskii, Phys. Status Solidi B **76**, 475 (1976).
[38] H. J. Herrmann, B. Derrida, and J. Vannimenus, Phys. Rev. B **30**, 4080 (1984); B. Derrida, D. Stauffer, H. J. Herrmann, and J. Vannimenus, J. Phys. (France) Lett. **44**, L701 (1983).
[39] F. Mallamace, S. H. Chen, Y. Liu, L. Lobry, and N. Micali, Physica A **266**, 123 (1999).